

# Towards Generalising Neural Implicit Representations

Theo W. Costain Victor Adrian Prisacariu

Active Vision Lab

Department of Engineering Science

University of Oxford, UK

{theo,victor}@robots.ox.ac.uk

**Abstract**—Neural implicit representations have shown substantial improvements in efficiently storing 3D data, when compared to conventional formats. However, the focus of existing work has mainly been on storage and subsequent reconstruction. In this work, we argue that training neural representations for both reconstruction tasks, alongside conventional tasks, can produce more general encodings that admit equal quality reconstructions to single task training, whilst providing improved results on conventional tasks when compared to single task encodings. Through multi-task experiments on reconstruction, classification, and segmentation our approach learns feature rich encodings that produce high quality results for each task. We also reformulate the segmentation task, creating a more representative challenge for implicit representation contexts.

## I. INTRODUCTION

Implicit neural representations have garnered significant interest recently for their ability to reconstruct complex 3D structures and shapes. The appeal of these methods stems from a number of useful properties they possess for both reconstructing 3D shapes, as well as storing them efficiently. By learning the reconstruction of the shapes, networks are able to encode and use a rich set of priors over the 3D domain to improve the quality of the reconstructions over what can be achieved with classical methods[20, 23]. Efficiency in storage is achieved by decoupling the encoding from the input and output modality so, unlike voxel based representation, the storage requirements do not grow cubically with the output resolution. Further, implicit representations do not suffer from the limitations of mesh and point-cloud based representations, where the quality of the reconstruction is typically limited by the output size constraints of a single feed forward pass[20].

Conditioning a “decoder” network on an encoded representation of the input data, neural representations query the network at sample point locations for occupancy or distance function information. This approach allows for reconstructions to be generated with arbitrary resolutions at run-time[20].

Whilst these properties are impressive, we argue that further useful properties have been left on the table. In many of the works making use of implicit methods, training is performed with the loss function targeted only at reconstruction accuracy. This approach, whilst clearly effective, misses a significant potential benefit. We argue that using a multi task loss, including loss terms related to common tasks such as classification, produces encodings that are equally effective for

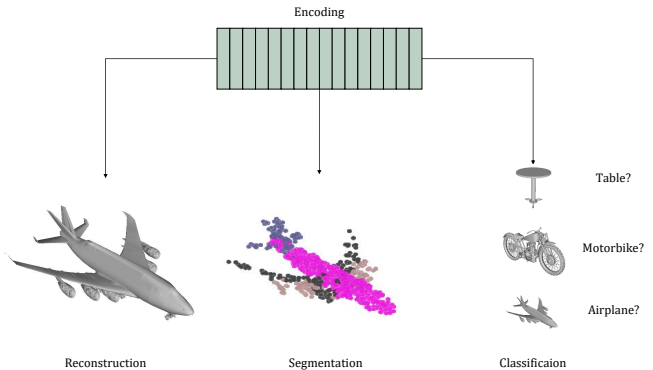


Fig. 1. Through multi-task training, implicit representations can be enriched creating a more general representation of a shape or object, and allowing for their use in a number of tasks rather than simply reconstruction.

reconstruction, but that still provide a richer set of features for use in other downstream tasks. We suggest that in applications such as augmented reality, where efficient representations are very useful, the ability to encode more than just shape information into the representation is likely to be useful.

Whilst a number of works have produced impressive and high quality reconstructions using a number of different approaches, there is a general aim in the design neural network encoders to produce features that have meaningful uses beyond a single task. However, we observe that this aim has not yet translated to implicit representation works. Many practical applications of implicit representations to real world problems would benefit from the ability to perform multiple tasks using the same stored data, rather than having to render and re-encode before performing other downstream tasks.

In this paper, we examine the generation of more descriptive neural representation encodings. Through experiments, we show that encodings generated purely for reconstruction can produce poorer results on other tasks. Further, we show clearly that the encodings used in neural representations can be trained to develop properties useful for other tasks common in computer vision, without any appreciable reduction in reconstruction performance. Whilst this should be possible for any number of tasks or applications such as texture generation, material property estimation, we examine two common tasks in 3D, namely classification and segmentation. We also argue

that the conventional 3D semantic segmentation task does not translate well to implicit representations, where the object being reconstruction is not or cannot be operated on directly. To address this we propose, among other experiments, a re-formulation of the semantic segmentation task that is a more representative formulation of the segmentation task when applied to implicit representations.

In summary, the key contributions of this paper are

- A simple extension to existing implicit representation approaches allowing the simultaneous training of reconstruction, segmentation and classification in a multi-task fashion.
- Experiments showing implicit encodings can admit substantially improved performance on common computer vision tasks, without any compromise to reconstruction accuracy.
- A re-formulation of the semantic segmentation task, that is more representative of a real world task in the context of implicit representations.

## II. RELATED WORK

Implicit or Neural representations have been the subject of much recent work. Early works primarily focused on single objects[2, 10, 11, 20, 21, 23, 26, 29, 30, 37], encoding some input, often either image or point-cloud, and producing a feature vector which is used to condition the output network. There have been different approaches to conditioning the network with concatenation, however they mainly fall into two categories: i) concatenation/biasing (Dumoulin et al. [9] argue that biasing and concatenation are analogous) and ii) hyper-networks. Further, the implementation of the implicit representation can be divided into two categories, namely occupancy generating functions or signed distance function (SDF) generating functions<sup>1</sup>. In concatenation based conditioning, the encoding is concatenated with the point being queried and then passed through the network. In hyper-networks, the encodings is passed through a small network, whose outputs are the weights used in the network that actually predicts the value for a given query point.

Early works such as [20, 23, 29] showed that simple MLP networks were capable of representing complex distance functions and occupancy functions. Park et al. [23] also detailed the use of auto-decoders to estimate optimal encodings for a given input, using a fixed decoder and simple backpropagation. Mescheder et al. [20] first demonstrated the alternative occupancy paradigm for implicit representations, as well as proposing a procedure to extract high quality meshes in an efficient manner from the implicit representation, using an octree like approach. Michalkiewicz et al. [21] learn level sets to represent shapes. We note that the level sets are equivalent to learning an unsigned distance function like Atzmon and Lipman [2]. Poursaeed et al. [26] combines both explicit

<sup>1</sup>Arguably occupancy networks are simply SDF networks with the sign function applied to their output, however this ignores the increased complexity in regressing SDF values rather than simply their sign. We argue this point in more detail in Sec. III-A

atlas based reconstruction and implicit neural reconstruction, enforcing consistency between the two methods.

Later works investigated larger scenes[3, 24], however many of these methods did not expand the size of the area described by a given embedding, instead proposing methods to recover encodings for a small local region where a neural representation can then extract shape information. Peng et al. [24] interpolated between encoded points in a volume or plane, to generate the conditioning vector for a occupancy network in a region around the encoded point. Chibane et al. [5] took a similar approach, adding also multiple resolutions of encoded volumes. A separate group of works[3, 14, 34] all took a slightly different approach from above and divided the scene into regions generating a small encoding for each region. Both [14] and [3] make use of a grid of small local encodings, whereas [34] make use of a number of oriented spherical patches of differing radii each with an encoding.

Further improvements to implicit representations in general were proposed by Sitzmann et al. [31] and Tancik et al. [32] showing that adding higher frequency information to simple networks, drastically improved their ability to generate high quality reconstructions. Duan et al. [8] proposed a curriculum based learning approach for implicit representations, improving reconstruction quality of complex local details.

Other works have used implicit representations for a number of other tasks, most notably novel view synthesis[18, 22, 28].

There have also been a number of works considering the application of multi-task approaches to 3D problems[12, 16, 17, 25]. Multi-task learning has enabled improvements where tasks are related or closely coupled, such as semantic and instance segmentation[16, 25]. As well Hassani and Haley [12], made use of a multi-task setup in unsupervised training to learn an embedding space over 3D point-cloud inputs.

To our knowledge, only one other paper has investigated using implicit representations for tasks other than reconstruction[15]. However, their work focused only on the 2D domain (albeit using an internal 3D modality), prohibiting any meaningful comparison with our method.

## III. METHOD

In this section, we first cover the principles of implicit representations. We then describe the other tasks we consider, including our variation to the normal task of segmentation that we use in our experiments for a fairer representation of the segmentation task in an implicit context. Finally we discuss our network architecture and training procedure.

### A. Implicit Representations

Neural implicit representations attempt to estimate the function describing the surface of a given object. A common formulation is to map from a point,  $\mathbf{p} \in \mathbb{R}^3$ , in space to the smallest signed distance between the point and the outer face of a surface, *i.e.* a SDF. This gives rise to an expression[23, 37] of the form

$$s : \mathbb{R}^3 \rightarrow \mathbb{R}$$

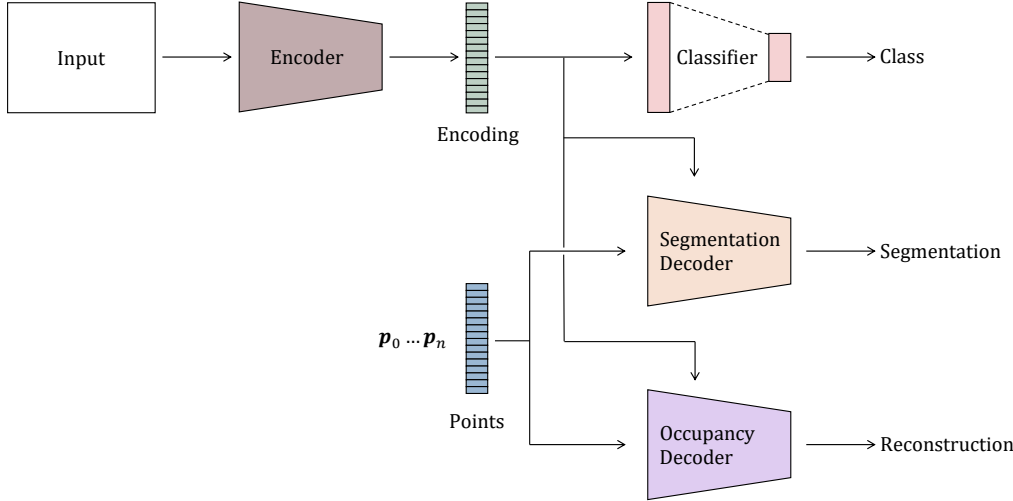


Fig. 2. An overview of our network architecture. The network takes as input either images or point-clouds, generating an encoding from them. This encoding can then be used in a number of ways. For classification, the encoding is passed directly into a simple classifier. For segmentation and reconstruction, the encoding is used to condition the decoder networks. The decoder networks take a number of points as input and returns for each point either, the probability that that point lies inside the encoded shape, or semantic label probabilities.

Another common formulation is to estimate the probability that a given point lies within the object (*i.e.* probability of occupancy), rather than regressing the SDF directly. This gives a function[20] of the form

$$o : \mathbb{R}^3 \rightarrow \{0, 1\}$$

However, we note the following relationship

$$o = \sigma(-s) > \tau \quad (1)$$

where  $\tau$  is a threshold parameter. This relationship suggests that the occupancy function is a simplified version of the SDF, moving the problem from a regression context and into a classification context. Further, this reformulation suggests that where the extra information provided by the SDF (but not the occupancy function) such as the surface normal (given as,  $\frac{\partial s}{\partial p}$ , the spatial gradient of the SDF[23]) is not needed, the occupancy function is likely to be easier to learn. If this is true, we suggest this is the result of the occupancy network only needing to learn a decision boundary over  $\mathbb{R}^3$  rather than having to learn both the boundary and then regress a points distance from it. Further, we note that papers using the SDF formulation do not actually measure the accuracy of the overall learnt SDF, instead they make use of metrics that compare rendered meshes with ground truth [21, 23, 30, 37]. The absence of metrics comparing the overall accuracy of the SDFs leaves open the possibility that the values of the implicit SDF are accurate only near the boundary region. Again, if this assertion is correct it would suggest that any difference in quality or output between SDF and occupancy formulations is minimal. Given this and the simplicity of the method, we

chose to use the formulation of Mescheder et al. [20] for our experiments.

### B. Other Tasks

The conventional 3D segmentation task as explored in a number of papers[27, 36] typically involves predicting a semantic label for each point in an given input point-cloud. However, in the context of implicit representations, this task loses much of its meaning. Particularly when the input is a degraded and noisy point-cloud (see Sec. IV). As we are considering the occupancy of a given spatial location, it makes more sense to consider the task as determining the semantic label of regions within the shape.

Hence, given a mesh  $\mathcal{X}$ , for each vertex  $\mathbf{x} \in \mathcal{X}$  with a semantic label  $c_x$ , the semantic class of any location  $\mathbf{p} \in \mathbb{R}^3 \cap \mathcal{X}$  lying inside the mesh, has the semantic class of the nearest vertex of  $\mathcal{X}$ .

$$c_p = c_z \quad \text{where } z = \arg \min_{\mathbf{x}} \|\mathbf{p} - \mathbf{x}\|_2$$

This scheme has the same effect as producing a Voronoi partitioning of the space inside the mesh. Points that lie outside the mesh, are considered to be background and therefore have no valid semantic class. The segmentation task then becomes predicting the label of a point inside the shape according to the nearest neighbour assignment. During both training and inference, we evaluate the semantic label task at the same locations as the reconstruction task.

As well as segmentation, we also investigate the performance of our approach to the task of classification. Unlike the segmentation task which requires the implicit code to encode

information about the properties of spatial regions (similarly also with the reconstruction task), classification requires that the encodings allow simple classification networks to discriminate between them. Later experiments (see Sec. V-B and Sec. V-C), show that the requirements classification has for the encodings are noticeably different to segmentation and reconstruction.

Our results show that implicit representations can be encouraged to be more representative of objects, rather than merely encoding their shape. We focus on two particular tasks that are common tasks, but expect that generalising the encodings over further tasks is likely to also be possible.

### C. Architecture

An overview of our network architecture is shown in Fig. 2. Our network takes as input to the encoder, either point-clouds or images. Throughout all the following experiments, we use the same two encoders. One for point-cloud input, and another for image based input.

**Point-cloud input** We use the same variation on the original network from [27] as Mescheder et al. [20]. In this formulation, the fully connected (FC) layers normally present in the original network are replaced by residual FC blocks[13]. During training the network samples 300 points from the input point cloud and applies Gaussian noise ( $\sigma = 0.005$ ) before passing these into the encoder(identically to [20]).

**Image input** We use a pre-trained ResNet-18[13], followed by a linear layer to reduce the output dimension following [20].

The encoded features are then passed to a decoder. For decoding point locations into either occupancy values or semantic labels we use one or more of the following, depending on the task(s). For classification, the encoding is passed directly to the classifier.

**Occupancy Decoder** This is the same decoder used in [20]. The network takes a number of points  $p_0, p_1, \dots, p_n$  as input and uses conditional batchnorms[7], which take the encoding as their input, to condition the network.

**Classifier** A simple 2 layer MLP, that takes the encoding directly as input and returns class probabilities.

**Segmentation Decoder** The same network as the occupancy decoder but with a larger output channel dimension.

**Joint Segmentation and Occupancy Decoder** Also the same network as the occupancy decoder, however rather than two separate networks for each task, the same network performs both tasks simultaneously. The output is then sliced along the channel dimension to yield two tensors, one containing the occupancy probability, and another containing the semantic label probabilities.

The loss functions used depend on the task. For the reconstruction loss,  $\mathcal{L}_{\text{rec}}$ , we use binary cross entropy as in[20]. Both classification,  $\mathcal{L}_{\text{cls}}$ , and segmentation,  $\mathcal{L}_{\text{seg}}$ , use the cross

entropy loss. In the multi task settings, the losses were combined in a weighted linear fashion as

$$\mathcal{L}_{\text{tot}} = \mathcal{L}_{\text{rec}} + \lambda_{\text{cls}} \times \mathcal{L}_{\text{cls}} + \lambda_{\text{seg}} \times \mathcal{L}_{\text{seg}}$$

for all experiments  $\lambda_{\text{cls}} = \lambda_{\text{seg}} = 1.0$ . We use an ADAM optimiser with learning rate of  $10^{-4}$ .

Training for joint tasks takes approximately 4 days on an NVIDIA GeForce GTX 1080Ti.

## IV. EXPERIMENTS

Experiments are divided into three parts. First we consider the original dataset from [20], establishing a baseline and some preliminary experiments involving reconstruction and classification. Next we examine a more challenging classification task, before turning finally to a semantic segmentation task.

### A. Datasets

We perform our experiments on a number of datasets. The original dataset from Mescheder et al. [20] is the subset of ShapeNetCore[4] from Choy et al. [6]. We also make use of ModelNet40[35] for further classification experiments and ShapeNetPart[38] for our segmentation experiments. Data pre-processing pipelines were accelerated with GNU Parallel[33].

We limit our experiments to datasets with similar properties to those used in [20], as we are not seeking to validate the specific implicit representation format we are using, rather the benefits of more feature rich encodings. This means that we do not consider larger scale datasets such as Stanford3D[1] that our chosen method might struggle with. We leave this to future experiments with other methods such as [24] or [3] that are better able to reconstruct larger scenes.

For all experiments, the properties of the inputs remain constant. For point-clouds we sample 300 points from the ground truth point-cloud, and apply noise using a Gaussian distribution with zero mean and standard deviation 0.05 to the sampled point clouds, identically to [20]. For images we crop and resize the images identically to [20].

1) *Choy / ShapeNetCore*: The dataset used in Mescheder et al. [20] from which our work builds on, uses the renderings and voxelisations[6] of a subset of the ShapeNetCore[4] dataset. We use the rendered images to train the image based encoder in later experiments. The fully processed dataset was provided by [20] as part of their publication. Briefly, meshes are loaded and a large number of depth images are rendered. These depth images are fused to form a watertight mesh from which points and their corresponding occupancy value can be sampled. Although the occupancy samples are not provided as part of the dataset in[6], to reduce ambiguity we will refer to the dataset from [20] as the Choy dataset throughout this paper. The dataset consists of 30,648 training meshes, 4,358 validation meshes and 3,738 test meshes across 13 object categories.

We use the Choy dataset both for our baseline experiments, as well as some preliminary classification experiments. Whilst this dataset only contains 13 separate classes, this provides sufficient preliminary experiments to validate our hypothesis. Our experiments with this dataset are outlined in Sec. V-A.

TABLE I

EXPERIMENTS ON THE CHOY DATASET WITH POINT-CLOUD INPUT, SHOWING SHAPE IOU AND CLASSIFICATION ACCURACY. FOR THE CLASSIFICATION TASK WITH THE ONET ENCODER, THE ENCODER WAS FIXED TO ALLOW FOR THE CLASSIFICATION PERFORMANCE OF THE ENCODINGS THEM-SELVES TO BE EVALUATED.

	IOU	Chamfer L1	Accuracy
ONet baseline	0.78	0.0081	—
Classification baseline	—	—	0.92
Classification w/ ONet encoder	—	—	0.80
Joint Classification & ONet	0.77	0.0084	0.92

2) *ModelNet40*: For further classification experiments, we make use of the popular ModelNet40[35] dataset. As rendered images were not readily available, we rendered images using Pyrender[19] in the same fashion as [6], choosing 24 viewpoints with constant radius and altitude, but random azimuth. The occupancy samples are generated with the code provided by [20]. The dataset consists of 9,843 training meshes and 2,468 testing meshes across 40 object categories. Our experiments with this dataset are outlined in Sec. V-B.

3) *ShapeNetPart*: For our semantic segmentation experiments, we make use of the dataset from Yi et al. [38], which we refer to as ShapeNetPart. Again the occupancy samples were generated using the code from [20]. Semantic labels were assigned to the occupancy samples using a simple nearest neighbour assignment from the ground truth semantic labels in[38]. The dataset consists of 12,121 training, 1,854 validation, and 2,858 testing meshes following the corresponding splits from ShapeNetCore. Our experiments with this dataset are outlined in Sec. V-C.

## V. RESULTS

### A. Choy Experiments

We begin with the dataset from the original paper. Our experiments with point-cloud input are shown in Table I. Given the small number of classes and fairly unique visual properties of the classes in this dataset, the high accuracy in classification is not unexpected, even with the reduced quality of the input point-clouds. To evaluate the performance of baseline encoder, we fix the encoder and train a simple classifier on the output. This classifier shows a substantial reduction in accuracy, compared to the jointly trained classification and reconstruction results, where the full accuracy on both tasks was recovered. For the jointly trained experiment, the encoder was *not* fixed.

Our experiments with image input are shown in Table II. The results are similar to the point-cloud experiments. As discussed in [20], the lower performance in reconstruction for the ONet can potentially be attributed to occlusion. We do not include the “Classification with ONet encoder” experiment, as the encodings from the pre-trained ResNet are likely already effective for classification, meaning this experiment is not likely to provide any new insight. The joint training result shows that the encoding is capable of performing both tasks without loss of accuracy.

TABLE II

EXPERIMENTS ON THE CHOY DATASET WITH IMAGE INPUT, SHOWING SHAPE IOU AND CLASSIFICATION ACCURACY.

	IOU	Chamfer L1	Accuracy
ONet baseline	0.58	0.021	—
Classification baseline	—	—	0.92
Joint Classification & ONet	0.59	0.020	0.92

TABLE III

EXPERIMENTS ON THE MODELNET40 DATASET WITH POINT-CLOUD INPUT, SHOWING SHAPE IOU AND CLASSIFICATION ACCURACY. AS IN TABLE I, THE ENCODER FOR THE CLASSIFICATION WITH ONET ENCODER WAS FIXED.

	IOU	Chamfer L1	Accuracy
ONet baseline	0.73	0.011	—
Classification baseline	—	—	0.82
Classification w/ ONet encoder	—	—	0.57
Joint Classification & ONet	0.70	0.012	0.82

### B. ModelNet40 Experiments

To better evaluate the classification performance, as well as the shortcomings of the reconstruction encodings in classification, we run the same experiments as in Sec. V-A on ModelNet40, a more conventional 3D classification benchmark.

Our experiments with point-cloud input are shown in Table III. The results follow a similar pattern to the point-cloud results from the Choy dataset. As we expected, when we train the classifier using the fixed encoder from the reconstruction task, the classification performance is poor. This reduction in performance is much more severe than on the Choy dataset, but is consistent with the increased difficulty shown by the lower accuracy figure on the classification baseline. However, this performance loss is completely recovered in the joint training, with only a minor decrease in reconstruction performance.

Our experiments with image input are shown in in Table IV. Here we see that the joint training is able to recover much of the performance on either of the single tasks. Again, because of the nature of the pre-trained ResNet, we do not include the fixed encoder task.

### C. ShapeNetPart Experiments

Our metric for the segmentation task is mean average Intersection over Union (mIOU). Points are sampled within the shape and assigned semantic labels by the decoder. The same sample points are used for both segmentation and reconstruction. Whilst in a real world scenario points would be

TABLE IV  
EXPERIMENTS ON THE MODELNET40 DATASET WITH IMAGE INPUT, SHOWING SHAPE IOU AND CLASSIFICATION ACCURACY.

	IOU	Chamfer L1	Accuracy
ONet baseline	0.54	0.034	—
Classification baseline	—	—	0.85
Joint Classification & ONet	0.51	0.036	0.84

TABLE V

EXPERIMENTS ON THE SHAPENETPART DATASET WITH POINTCLOUD INPUT, SHOWING SHAPE IOU, SEGMENTATION MIOUT, AND CLASSIFICATION ACCURACY.

	IOU	Chamfer L1	mIOU	Accuracy
ONet baseline	0.69	0.010	—	—
Classification baseline	—	—	—	0.95
Segmentation baseline	—	—	0.53	—
Segmentation w/ ONet encoder	—	—	0.49	—
Joint Segmentation & ONet	0.70	0.0098	0.50	—
Parallel Segmentation & ONet	0.68	0.011	0.53	—
Joint Segmentation & Classification & ONet	0.72	0.0086	0.50	0.95

sampled both inside and outside the shape, we wish to assess the performance of the segmentation decoder independently of the reconstruction performance, and so only consider points inside the shape. The IOU computed is for each part in each shape, and averaged to give a shape IOU. If there are no ground truth points for a given part (*e.g.* whilst armrest is a part of the chair class, many of the chair instances do not have arms), then the part is automatically assigned an IOU of 1. We can then compute mIOU as the average of the shape IOUs. At inference, time points are sampled randomly from a padded bounding box of the ground truth object, as in [20].

Table V shows the reconstruction accuracy, mIOU and classification accuracy of our different experiments on the ShapeNetPart dataset. The results show little to no accuracy being lost in any of the tasks for the jointly trained settings. Unlike in Table III with the fixed encoder, segmentation with a fixed ONet encoder does not show significantly worse performance than the baseline task. We suggest that this might be due to similarities between the reconstruction task and our modified segmentation task. In the reconstruction task, the network is attempting to learn an encoding that represents the shape properties of a given region of space, such as the curvature and boundaries. These properties are likely also useful for the task of segmentation, *i.e.* the semantic class probabilities are potentially dependant on properties like local curvature.

Table V shows the per-class segmentation results for the baseline, fixed encoder and joint training as well as the reconstruction IOU for the baseline. The poor performance on some of the classes such as rocket and headphones may be explained by the thin sections in parts of those objects. Because the network samples points within the shapes randomly, thin sections like the fins(rocket), cable(earphones), or handlebar(motorbike) are likely to be undersampled and therefore have poor performance at inference time (see Fig 3). As well as this imbalance, there is also significant imbalance in the number of models in certain categories which can negatively affect accuracy at inference time. This is reflected in the higher mIOU scores across all the experiments, for the classes with more shapes.

Fig. 4 shows some selected qualitative segmentation results. The segmentation decoders show good results for bulk areas like the wings and body on the aeroplane(1st row) and simple objects like the guitar(4th row). However areas like the chair arms(3rd row) present more of a challenge. We can also see another example of the low performance of thin sections on the roofs of the cars(2nd row), particularly so for the right hand car.

Fig. 3 shows some of the failure cases of the segmentation decoder. A particularly extreme case (2nd row) is shown where the correct semantic labels are completely inverted.



Fig. 3. Segmentation failure cases. Ground truth on the left, predicted segmentation on the right. For the rocket, thin features like the fins can be under-sampled and therefore confuse the network. The cable on the earphones may also suffer from this problem. The earphones present a complete failure with semantic classes completely inverted.

## VI. CONCLUSION

In this paper we have discussed the potential to generalise the encodings used by implicit representations to a broader range of tasks. We discuss the current narrow focus of implicit representations, and the potential issues this raises for applications of implicit representations in the real world. We also introduce a modified formulation of the conventional segmentation task that is more applicable to implicit contexts, and detail an appropriate network to use for this new formulation. We choose two common computer vision tasks and demonstrate that through multi-task training, we can enrich the encodings achieving strong performance across the tasks without any loss in reconstruction accuracy, also showing how certain encodings can struggle with some tasks but not others.

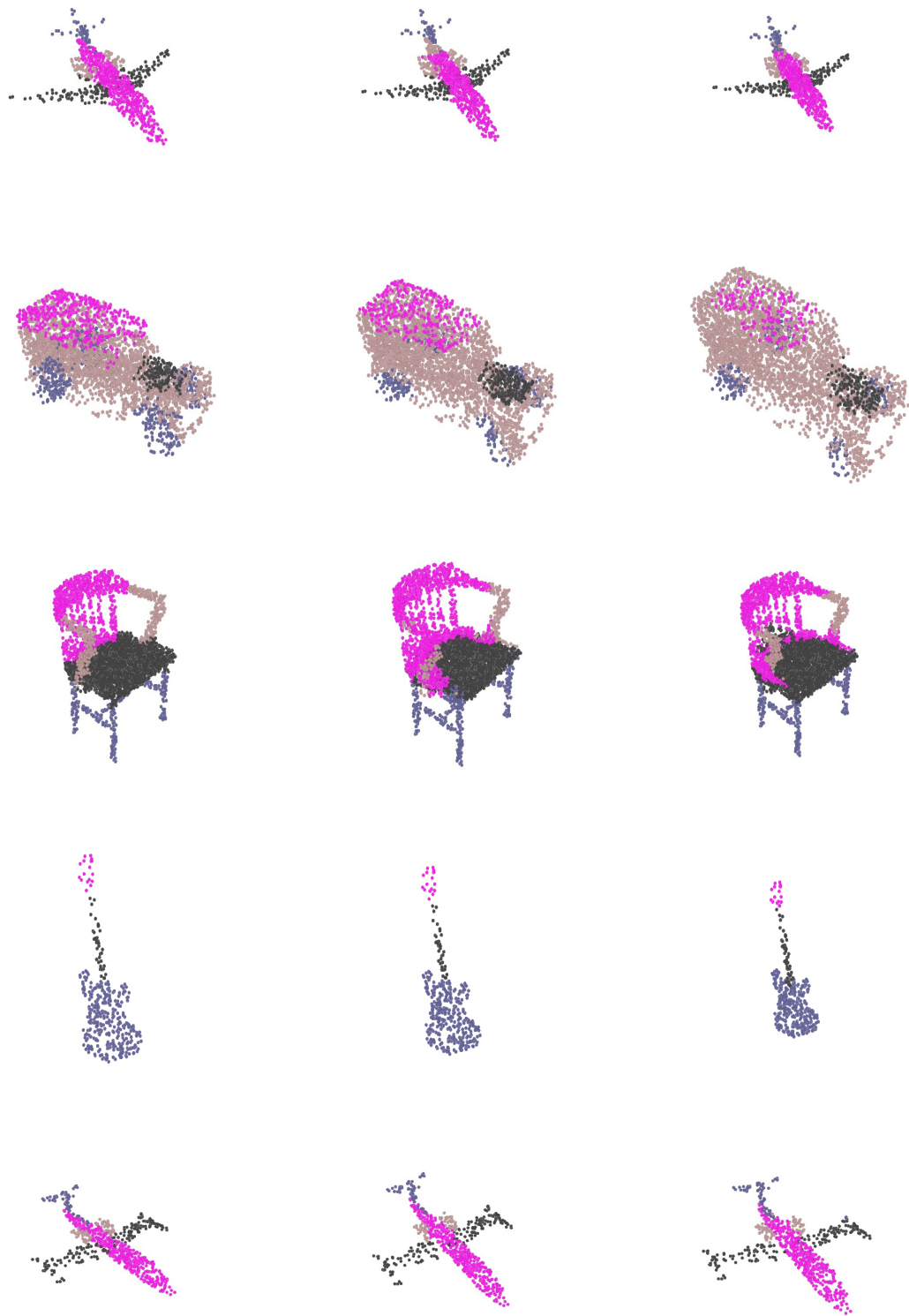


Fig. 4. Qualitative segmentation results on the ShapeNetPart[38] dataset. From left to right: Ground truth, Segmentation baseline, Joint segmentation and classification and ONet.

TABLE VI

EXPERIMENTS ON THE SHAPENETPART DATASET WITH POINT-CLOUD INPUT, DETAILING PER CLASS RESULTS, SHOWING SEGMENTATION MIOU.

Class	ONet (reconstruction IOU)	Segmentation	Segmentation w/ ONet encoder	Joint Segmentation & ONet	Parallel Segmentation & ONet	Joint Segmentation & Classification & ONet
Airplane	0.75	0.586	0.539	0.552	0.588	0.55
Bag	0.708	0.464	0.445	0.455	0.496	0.42
Cap	0.555	0.446	0.379	0.403	0.45	0.381
Car	0.798	0.523	0.5	0.505	0.528	0.494
Chair	0.7	0.628	0.585	0.619	0.632	0.62
Earphone	0.559	0.314	0.276	0.305	0.332	0.322
Guitar	0.751	0.679	0.657	0.662	0.684	0.659
Knife	0.705	0.549	0.5	0.533	0.557	0.536
Lamp	0.542	0.519	0.466	0.486	0.524	0.49
Laptop	0.81	0.589	0.594	0.588	0.595	0.591
Motorbike	0.527	0.53	0.431	0.468	0.528	0.446
Mug	0.758	0.576	0.554	0.533	0.575	0.545
Pistol	0.754	0.588	0.573	0.562	0.598	0.558
Rocket	0.726	0.385	0.365	0.295	0.392	0.299
Skateboard	0.684	0.508	0.479	0.469	0.504	0.458
Table	0.703	0.567	0.535	0.564	0.568	0.56
Mean	0.689	0.528	0.493	0.5	0.535	0.496

## REFERENCES

- [1] I. Armeni, O. Sener, A. R. Zamir, H. Jiang, I. Brilakis, M. Fischer, and S. Savarese. 3d semantic parsing of large-scale indoor spaces. In *Proceedings of the IEEE Conference on Computer Vision and Pattern Recognition*, pages 1534–1543, 2016. [4](#)
- [2] M. Atzmon and Y. Lipman. Sal: Sign agnostic learning of shapes from raw data. In *Proceedings of the IEEE/CVF Conference on Computer Vision and Pattern Recognition*, pages 2565–2574, 2020. [2](#)
- [3] R. Chabra, J. E. Lenssen, E. Ilg, T. Schmidt, J. Straub, S. Lovegrove, and R. Newcombe. Deep local shapes: Learning local sdf priors for detailed 3d reconstruction. *arXiv preprint arXiv:2003.10983*, 2020. [2, 4](#)
- [4] A. X. Chang, T. Funkhouser, L. Guibas, P. Hanrahan, Q. Huang, Z. Li, S. Savarese, M. Savva, S. Song, H. Su, J. Xiao, L. Yi, and F. Yu. ShapeNet: An Information-Rich 3D Model Repository. Technical Report arXiv:1512.03012 [cs.GR], Stanford University — Princeton University — Toyota Technological Institute at Chicago, 2015. [4](#)
- [5] J. Chibane, T. Alldieck, and G. Pons-Moll. Implicit functions in feature space for 3d shape reconstruction and completion. In *Proceedings of the IEEE/CVF Conference on Computer Vision and Pattern Recognition*, pages 6970–6981, 2020. [2](#)
- [6] C. B. Choy, D. Xu, J. Gwak, K. Chen, and S. Savarese. 3d-r2n2: A unified approach for single and multi-view 3d object reconstruction. In *European conference on computer vision*, pages 628–644. Springer, 2016. [4, 5](#)
- [7] H. De Vries, F. Strub, J. Mary, H. Larochelle, O. Pietquin, and A. C. Courville. Modulating early visual processing by language. In *Advances in Neural Information Processing Systems*, pages 6594–6604, 2017. [4](#)
- [8] Y. Duan, H. Zhu, H. Wang, L. Yi, R. Nevatia, and L. J. Guibas. Curriculum deep sdf. *arXiv preprint arXiv:2003.08593*, 2020. [2](#)
- [9] V. Dumoulin, E. Perez, N. Schucher, F. Strub, H. d. Vries, A. Courville, and Y. Bengio. Feature-wise transformations. *Distill*, 2018. doi: 10.23915/distill.00011. <https://distill.pub/2018/feature-wise-transformations>. [2](#)
- [10] K. Genova, F. Cole, D. Vlasic, A. Sarna, W. T. Freeman, and T. Funkhouser. Learning shape templates with structured implicit functions. In *Proceedings of the IEEE International Conference on Computer Vision*, pages 7154–7164, 2019. [2](#)
- [11] A. Gropp, L. Yariv, N. Haim, M. Atzmon, and Y. Lipman. Implicit geometric regularization for learning shapes. *arXiv preprint arXiv:2002.10099*, 2020. [2](#)
- [12] K. Hassani and M. Haley. Unsupervised multi-task feature learning on point clouds. In *Proceedings of the IEEE International Conference on Computer Vision*, pages 8160–8171, 2019. [2](#)
- [13] K. He, X. Zhang, S. Ren, and J. Sun. Deep residual learning for image recognition. In *Proceedings of the IEEE conference on computer vision and pattern recognition*, pages 770–778, 2016. [4](#)
- [14] C. Jiang, A. Sud, A. Makadia, J. Huang, M. Nießner, and T. Funkhouser. Local implicit grid representations for 3d scenes. In *Proceedings of the IEEE/CVF Conference on Computer Vision and Pattern Recognition*, pages 6001–6010, 2020. [2](#)
- [15] A. Kohli, V. Sitzmann, and G. Wetzstein. Inferring semantic information with 3d neural scene representations. *arXiv preprint arXiv:2003.12673*, 2020. [2](#)
- [16] J. Lahoud, B. Ghanem, M. Pollefeys, and M. R. Oswald. 3d instance segmentation via multi-task metric learning. In *Proceedings of the IEEE International Conference on Computer Vision*, pages 9256–9266, 2019. [2](#)
- [17] M. Liang, B. Yang, Y. Chen, R. Hu, and R. Urtasun. Multi-task multi-sensor fusion for 3d object detection. In *Proceedings of the IEEE Conference on Computer Vision and Pattern Recognition*, pages 7345–7353, 2019. [2](#)
- [18] R. Martin-Brualla, N. Radwan, M. S. Sajjadi, J. T. Barron, A. Dosovitskiy, and D. Duckworth. Nerf in the wild: Neural radiance fields for unconstrained photo collections. *arXiv preprint arXiv:2008.02268*, 2020. [2](#)
- [19] M. Matl. Pyrender, 2020. URL <https://github.com/mmatl/pyrender>. (Version 0.1.43). [5](#)
- [20] L. Mescheder, M. Oechsle, M. Niemeyer, S. Nowozin, and A. Geiger. Occupancy networks: Learning 3d reconstruction in function space. In *Proceedings of the IEEE Conference on Computer Vision and Pattern Recognition*, pages 4460–4470, 2019. [1, 2, 3, 4, 5, 6](#)
- [21] M. Michalkiewicz, J. K. Pontes, D. Jack, M. Baktashmotlagh, and A. Eriksson. Deep level sets: Implicit surface representations for 3d shape inference. *arXiv preprint arXiv:1901.06802*, 2019. [2, 3](#)

[22] B. Mildenhall, P. P. Srinivasan, M. Tancik, J. T. Barron, R. Ramamoorthi, and R. Ng. Nerf: Representing scenes as neural radiance fields for view synthesis. *arXiv preprint arXiv:2003.08934*, 2020. 2

[23] J. J. Park, P. Florence, J. Straub, R. Newcombe, and S. Lovegrove. Deepsdf: Learning continuous signed distance functions for shape representation. In *Proceedings of the IEEE Conference on Computer Vision and Pattern Recognition*, pages 165–174, 2019. 1, 2, 3

[24] S. Peng, M. Niemeyer, L. Mescheder, M. Pollefeys, and A. Geiger. Convolutional occupancy networks. In *European Conference on Computer Vision (ECCV)*, Cham, Aug. 2020. Springer International Publishing. 2, 4

[25] Q.-H. Pham, T. Nguyen, B.-S. Hua, G. Roig, and S.-K. Yeung. Jsis3d: joint semantic-instance segmentation of 3d point clouds with multi-task pointwise networks and multi-value conditional random fields. In *Proceedings of the IEEE Conference on Computer Vision and Pattern Recognition*, pages 8827–8836, 2019. 2

[26] O. Poursaeed, M. Fisher, N. Aigerman, and V. G. Kim. Coupling explicit and implicit surface representations for generative 3d modeling. *arXiv preprint arXiv:2007.10294*, 2, 2020. 2

[27] C. R. Qi, H. Su, K. Mo, and L. J. Guibas. Pointnet: Deep learning on point sets for 3d classification and segmentation. In *Proceedings of the IEEE conference on computer vision and pattern recognition*, pages 652–660, 2017. 3, 4

[28] V. Sitzmann, J. Thies, F. Heide, M. Nießner, G. Wetzstein, and M. Zollhofer. Deepvoxels: Learning persistent 3d feature embeddings. In *Proceedings of the IEEE Conference on Computer Vision and Pattern Recognition*, pages 2437–2446, 2019. 2

[29] V. Sitzmann, M. Zollhöfer, and G. Wetzstein. Scene representation networks: Continuous 3d-structure-aware neural scene representations. In *Advances in Neural Information Processing Systems*, pages 1121–1132, 2019. 2

[30] V. Sitzmann, E. R. Chan, R. Tucker, N. Snavely, and G. Wetzstein. Metasdf: Meta-learning signed distance functions, 2020. 2, 3

[31] V. Sitzmann, J. N. P. Martel, A. W. Bergman, D. B. Lindell, and G. Wetzstein. Implicit neural representations with periodic activation functions, 2020. 2

[32] M. Tancik, P. Srinivasan, B. Mildenhall, S. Fridovich-Keil, N. Raghavan, U. Singhal, R. Ramamoorthi, J. Barron, and R. Ng. Fourier features let networks learn high frequency functions in low dimensional domains. *Advances in Neural Information Processing Systems*, 33, 2020. 2

[33] O. Tange. Gnu parallel - the command-line power tool. *;login: The USENIX Magazine*, 36(1):42–47, Feb 2011. doi: <http://dx.doi.org/10.5281/zenodo.16303>. URL <http://www.gnu.org/s/parallel>. 4

[34] E. Tretschk, A. Tewari, V. Golyanik, M. Zollhöfer, C. Stoll, and C. Theobalt. Patchnets: Patch-based generalizable deep implicit 3d shape representations. In *European Conference on Computer Vision*, pages 293–309. Springer, 2020. 2

[35] Z. Wu, S. Song, A. Khosla, F. Yu, L. Zhang, X. Tang, and J. Xiao. 3d shapenets: A deep representation for volumetric shapes. In *Proceedings of the IEEE conference on computer vision and pattern recognition*, pages 1912–1920, 2015. 4, 5

[36] Y. Xie, J. Tian, and X. Zhu. A review of point cloud semantic segmentation. *IEEE Geoscience and Remote Sensing Magazine (GRSM)*, 2020. 3

[37] Q. Xu, W. Wang, D. Ceylan, R. Mech, and U. Neumann. Disn: Deep implicit surface network for high-quality single-view 3d reconstruction. In *Advances in Neural Information Processing Systems*, pages 492–502, 2019. 2, 3

[38] L. Yi, V. G. Kim, D. Ceylan, I.-C. Shen, M. Yan, H. Su, C. Lu, Q. Huang, A. Sheffer, and L. Guibas. A scalable active framework for region annotation in 3d shape collections. *ACM Transactions on Graphics (ToG)*, 35(6):1–12, 2016. 4, 5, 7